scientific reports

Check for updates

OPEN

Optimization design of support structure based on 3D printing technology

Zhang Guoqing[1]✉, Li Junxin[1], Zhou Xiaoyu[1] & Wang Anmin[2]

Parts are often warped and deformed when they are molded using selective laser melting (SLM) technology. Thus, it is necessary to study the addition support modes of parts molded using SLM. Consequently, we designed dendritic, E-stage and conical supports, having different structural parameters and different partitions using Magics, and then, we analyzed their performances using the finite element software Abaqus. The structural parameters of the supports were optimized and finally tested using SLM molding technology. The maximum stress concentration was found for dendritic supports, followed by E-stage supports, and then conical supports. The stress concentration and deformation level of Scheme 2 were less than those of Scheme 1. The stress intensity and deformation levels for two partitions were less than those for three partitions. For parts molded by SLM, the deformation was maximum for conical supports, followed by dendritic supports, and then E-stage supports. When gradient supports of similar volumes were added, additional partitions did not effectively improve the molding quality. When supports of similar volumes were added, adding gradient supports did not effectively improve the molding quality. The results provide a basis for the application of SLM in molding high-precision parts.

Keywords Selective laser melting, 316L alloy, Supporting structure, Warping deformation, Optimal design

Three-dimensional (3D) printing (additive manufacturing) technology adopts special software to slice and stratify a 3D model, revealing cross-section data, and then, rapid molding equipment is used to manufacture physical parts through the layer-by-layer superposition of materials. Owing to the use of layer-by-layer superpositioning, 3D printing technology can manufacture complex parts of almost any geometry, and it has the ability to process single pieces, small batches and complex geometries, producing finished parts with compact structures[1,2]. Selective laser melting (SLM) is a 3D printing technology that uses laser melting metal powder[3,4].

SLM molding technology does not require a fixture because it manufacturers parts through layer-by-layer superpositioning. However, during the manufacturing process, it is often necessary to add supports to guarantee the molding of parts. When parts are manufactured using SLM technology, supports play the following vital roles[5–8]: ① They hold the next layer of unmolded powder. When a large suspending part is molded, if there is no addition support for the applied metal powder, then the powder will collapse. During the processing of the next layer, when the powder brush spreads powder, the finished parts will be directly scraped away. When parts having a preexisting matrix and large suspension are molded, adhering slag will appear on the back of suspending parts, and the adhering slag will increase along with the suspension magnitude. If the suspension magnitude is too large, then the mold will fail; ② Because parts molded by SLM are characterized by rapid heating and cooling, a large shrinkage stress is generated inside the parts, making the parts warped and deformed. Supports connect the matrix and parts or the molded and unmolded parts, so as to pull parts and avoid warping and deformation; and ③ If there is no additional support when parts are molded by SLM, then the parts will be directly molded on the matrix. Consequently, they need to be removed using wire electrical discharge machining, which results in the parts losing their dimensional accuracy.

In view of the warping, deformation and collapse of parts molded by SLM, Lu et al.[9] analyzed and optimized part supports by simulating molding and found that thermally conductive supports effectively reduce part deformations. Reasonable hollow supports optimized the supporting structure to a certain extent, and heat treatments effectively lessen part deformation and residual stress. Chen Chao et al.[10] summarized the basic rules of manual support addition by analyzing the mechanisms of deformation in the molding process of suspending

[1]School of Mechanical and Electrical Engineering, Zhoukou Normal University, Zhoukou, Henan 466000, People's Republic of China. [2]School of Mechanical and Automotive Engineering, South China University of Technology, Guangzhou, Guangdong 510640, People's Republic of China. ✉email: zhangguoqing1202@sohu.com

structures using SLM, simulated deformation during the molding process of supporting structures and added parts manually and automatically to verify the correctness of the rules of support addition. Zhang Xiaochuan et al.[11] investigated the stress distribution law during the molding of suspending structures through experimentation and simulation, and they determined the design concept of non-uniform support distribution, designed a support layout based on the normal distribution and realized the optimized design of support distribution. Craeghs et al.[12] discovered that by generating more supporting structures, a more uniform distribution of temperature can be achieved, resulting in a smaller temperature gradient, better thermal conductivity and lower average temperatures. However, during the post-treatment stage, the supporting structures should be removed. Too many supporting structures wastes materials and increases production cost. Calignano et al.[13] derived an optimized combination of blocky supports using a Taguchi orthogonal array. Ehsan et al.[14] optimized the generation of supporting structures using geometric topology that took into account thermal conduction, and they generated supporting structures by using minimizing the heat dissipation weaknesses of supporting structures as the objective function, with a 3D topology optimization method. Our earlier studies revealed that[15] when adding supports having the same parameters as molded parts, if the latter have supporting chips for dividing non-tilted supports, then good molding effects are achieved. The warping and deformation degrees of parts grow linearly along with support height. Adding a 0°-tilted thermally conductive piecemeal support effectively reduces the warping and deformation of parts.

Currently, the types of additional support for parts molded by SLM, the contact area between supporting chips and physical parts and the addition of non-uniform supports have become research hotspots. The above studies partly improve the quality of parts molded by SLM. However, supports yielding better performances need to be studied. In this paper, the structures and addition modes of several popular supports were further optimized through simulation and actual part processing experiments, to enhance the molding quality of parts.

Materials and methods

Structural design of common supports

When complex parts are molded by SLM, supports are needed for the suspending surfaces of the parts to ensure molding quality. Dendritic, conical and E-stage supports are frequently used in SLM molding because of their good mechanical properties and limited required additions[16]. During SLM molding of physical parts with support, warping and deformation usually appear in the 2–3 layers where the molded parts contact the support. Therefore, to compare the performances of the above three support types, we designed a thin plate, 20 mm × 20 mm × 0.1 mm, in Magics, moved the thin plate to 10 mm above the processing platform and then independently added the above three support types having the same parameters, as shown in Fig. 1. The parameters of the conical support were as follows: the diameter of the conical apex was 0.1 mm, the diameter of conical base was 0.6 mm, the maximum row spacing between cones was 1.6 mm, the Z-axis offset was 0.05 mm, the part volume measured 40 mm^3, and the support volume was 171.286 mm^3. The parameters of the E-stage support were as follows: the length and width of top support were both 0.1 mm, the length and width of bottom support were both 0.5 mm, the influence area of the internal boundaries was 1 mm, the tilt angle of the bottom grid connector was 47.29°, the Z-axis offset was 0.05 mm, the part volume measured 40 mm^3, and the support volume was 357.873 mm^3. The parameters of the dendritic support were as follows: the diameter of the apex of the dendritic support was 0.1 mm, the diameter of base was 0.6 mm, the maximum row spacing of branches was 1.6 mm, the number of branches was set to 4, the Z-axis offset was 0.05 mm, the part volume measured 40 mm^3, and the support volume was 104.692 mm^3.

Manufacturing methods

The forming material of the proposed parts is 316L stainless steel powder (Britain SANDVIK Osprey Company). Its chemical composition meets the ASTM A276 requirement (Table 1). The average loose bulk density of 316L stainless steel powder is 4.66 g/cm^2, with an average flowability of 15.98 s/50 g. The particle size distribution is narrowly concentrated, with D10 at 22.24 μm, D50 at 34.66 μm, and D90 at 53.38 μm.

We used nitrogen as protective gas and controlled the oxygen content within 0.03%. The power of the machining laser was 170 W, the scanning speed was 500 mm/s, the hatch distance was 60 mm, and the machining layer thickness was 35 um. We applied an X–Y interlamination alteration scanning strategy.

Analysis methods

A thermal stress on parts with additional supports was analyzed using the finite element software Abaqus to judge the pros and cons of different structural supports and addition modes. In thermal conduction analysis, Abaqus determines the temperature distribution by solving the "energy conservation" equation. The simulation parameters were set as follows: the material was 316 L, the elastic modulus was $206e^9$ MPa, the Poisson's ratio was 0.3, and the coefficient of thermal expansion was $1.9e^{-5}$/℃. The initial temperature of predefined field support was set to 100 ℃, the heating mode was instantaneous heating, and the final temperature of predefined field part was set to 1,000 ℃. This temperature change differed from the actual change in the processing temperature, but this did not affect a comparison of the impacts of different support addition modes on the part's performance. The constraint mode was that of the support base. In this research, the pros and cons of different support addition modes were evaluated, and an optimized design was proposed, by comparing the stress concentrations and deformations of the parts.

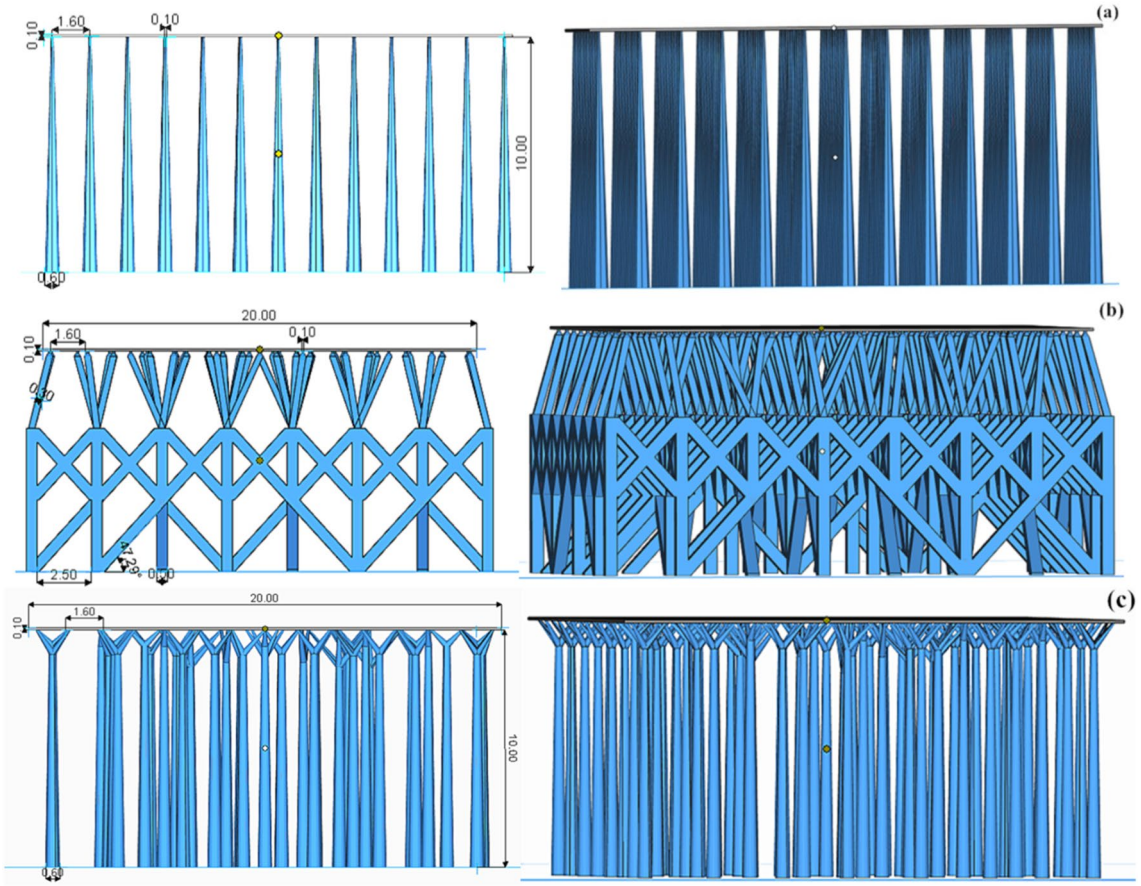

Figure 1. Schematic diagram of adding different structural supports to 0.1 mm thick thin plate: (**a**) Conical support; (**b**) E-Stage support and (**c**) Dendritic support.

Element	316 L Powder (%)	ASTM A276 Standard (%)	Element	316 L Powder (%)	ASTM A276 Standard (%)
C	< 0.03	< 0.03	Si	< 0.75	< 1.00
Mn	< 2.0	< 2.0	P	< 0.025	< 0.045
S	< 0.01	< 0.03	Cr	17.5–18	16–18
Ni	12.5–13	10–14	Mo	2.25–2.5	2–3
Cu	0.50	0.75	Fe	Balance	Balance

Table 1. The comparison of powder material manufactured in SLM and ASTM A276 standard.

Results and discussion

Thermal stress analysis of common supports

The stress and strain nephograms of a 0.1-mm thin plate added to different structural supports in Abaqus are shown in Fig. 2. As shown in Fig. 2 (a–c), the stress distribution areas of conical, E-stage and dendritic supports were basically the same, the stress was concentrated in the apices of the supports, and the stress intensity decreased progressively from apex to base. Nevertheless, the stress intensities of the above three supports differed slightly, with the maximum for the dendritic support being $1.45e^{10}$ MPa, followed by the E-stage support at $1.32e^{10}$ MPa, and the minimum stress intensity being that of the conical support at $9.09e^{9}$ MPa. As shown in the displacement nephograms of Fig. 2(d–f), the displacement distribution areas of conical, E-stage and dendritic supports were basically the same, the maximum displacements all appeared at the four corners of the 0.1 mm thin plate, and the maximum displacements of the supports also appeared at four corners, decreasing progressively from outside to inside. In addition, the maximum displacements of the three support types were slightly different, with the maximum for conical support at 0.241 mm, followed by the dendritic support at 0.136 mm, and the minimum displacement was that of the E-stage support at 0.119 mm. The conical support may have had the minimum stress concentration because it had a smooth gradient structure from top to bottom, allowing the stress to be well released. The E-stage support had a large transition between areas of upper and lower sections, whereas the dendritic support had a large transition between branches and crotches, which was not

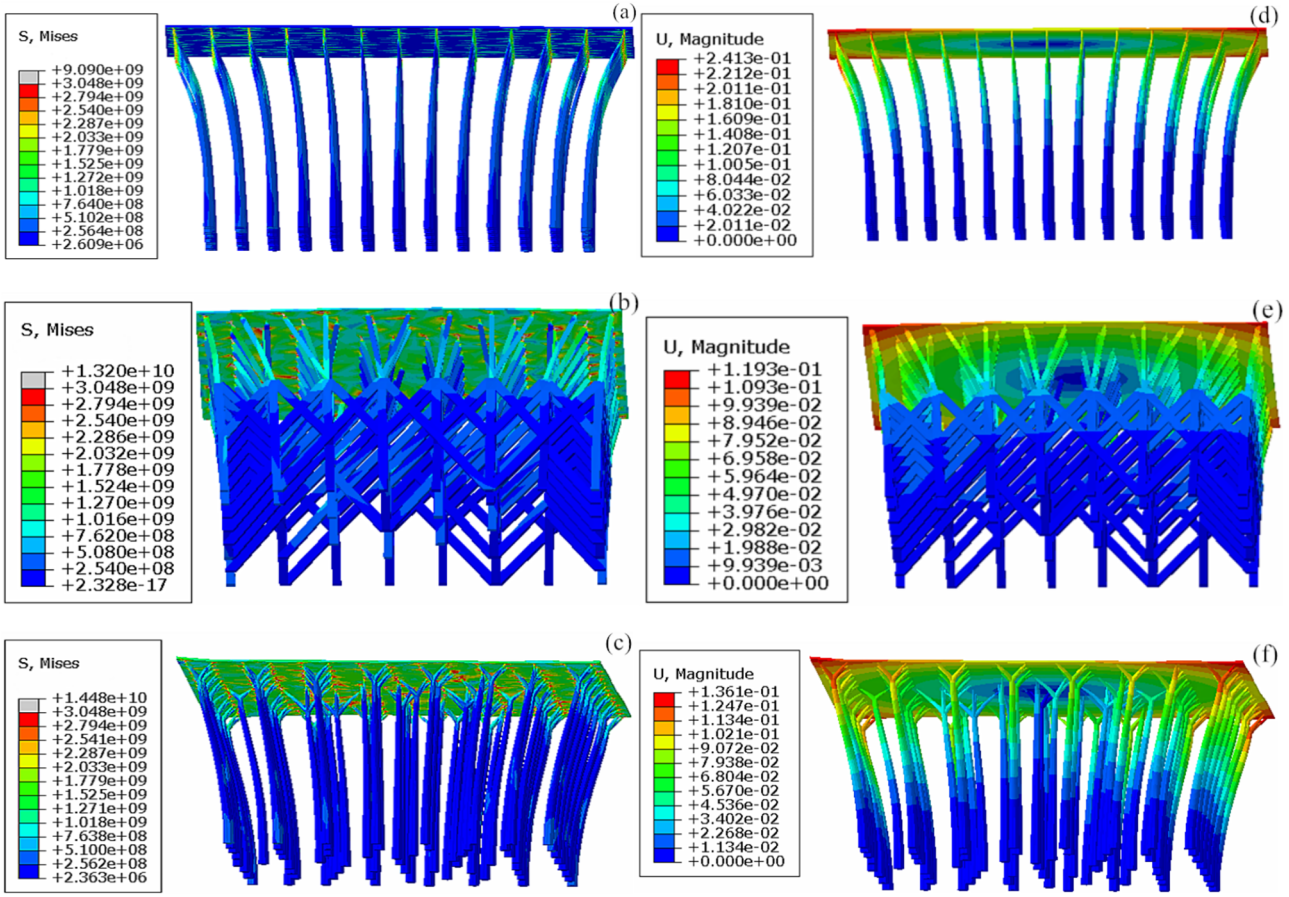

Figure 2. Stress–strain nephogram of 0.1 mm thick thin plate with different structural supports: (**a**) and (**d**) are conical supports; (**b**) and (**e**) are e-Stage supports; (**c**) and (**f**) are dendritic supports.

conducive to the release of stress. When SLM molding technology was used to manufacture parts, the smaller the part deformations, the better, as long as the support did not break. Therefore, the displacement analysis results allowed us to speculate that, barring the support breaking, E-stage supports had the best performances, followed by dendritic supports and then conical supports. However, E-stage supports require a large additional support volume (357.873 mm^3), which increased the processing time and cost of the parts. Thus, they are not practical when processing precious metals or the processing schedule is constrained. The volume of the dendritic support was only 104.692 mm^3, and it also resulted in small part deformations. Thus, we attempted to optimize the support design to minimize stress concentrations and deformations.

Analysis of the influence of changes in structural parameters on the performance of dendritic support

Design of dendritic supports with different structural parameters

To compare the influence of changes in structural parameters on the performance of dendritic supports, we designed a thin 20 mm × 20 mm × 0.1 mm plate in Magics, moved the thin plate to 10 mm above the processing platform and then independently added two dendritic supports having different parameters, as shown in Fig. 3. Scheme 1: The diameter of conical apex was 0.1 mm, the diameter of conical base was 0.6 mm, the maximum row spacing between cones was 1.6 mm, the Z-axis offset was 0.05 mm, the maximum trunk height was 8 mm, the number of branches was 4, the part volume measured 40 mm^3, and the support volume was 95.611 mm^3 (Fig. 3a). Scheme 2: The diameter of conical apex was 0.1 mm, the diameter of conical base was 0.6 mm, the maximum row spacing between cones was 1.6 mm, the Z-axis offset was 0.05 mm, the maximum trunk height was 8 mm, the number of branches was 4, a breaking point was added in the vertical direction (0.3 mm in diameter and 1 mm from the top), the part volume measured 40 mm^3, and the support volume was 112.672 mm^3 (Fig. 3b).

Thermal stress analysis of dendritic supports with different structural parameters

The stress and strain nephograms of dendritic supports having different structural parameters are shown in Fig. 4. As shown in Fig. 4(a) and (b), the stress distribution areas of dendritic supports having different structural parameters all appeared at the apices of supports, and the stress intensity decreased progressively from apex to base. The stress distribution areas of Scheme 2 were more uniform than those of Scheme 1. The stress intensity distribution was $2.072e^{10}$ MPa for Scheme 1 and $8.272e^{9}$ MPa for Scheme 2, and the value for Scheme 2 was lower

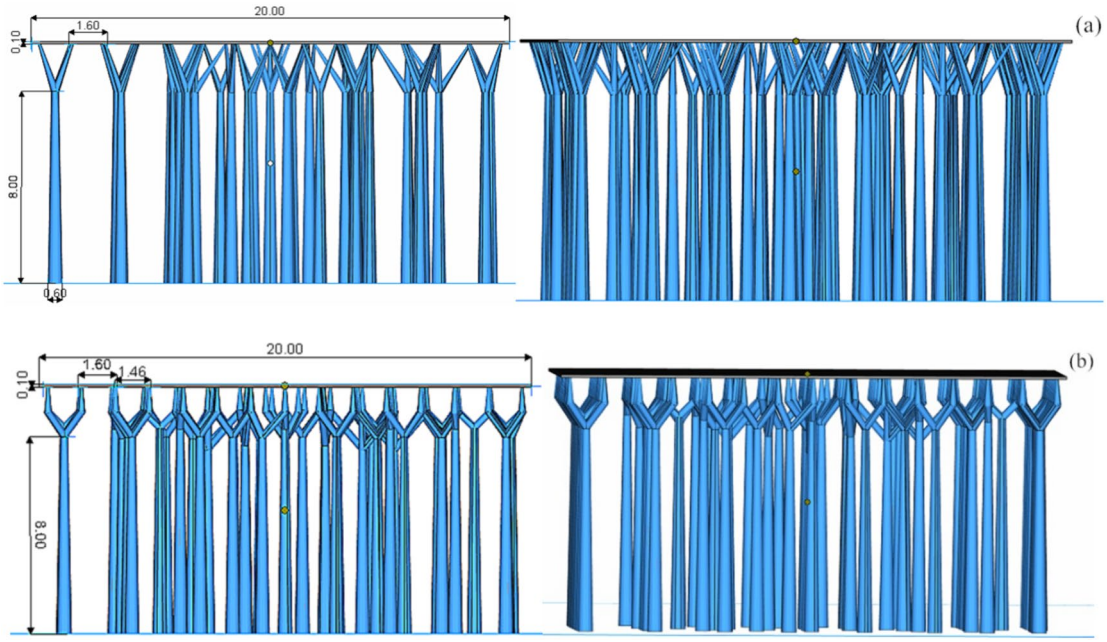

Figure 3. Schematic diagram of adding different structural supports to 0.1 mm thick thin plate: (**a**) Scheme 1; (**b**) Scheme 2.

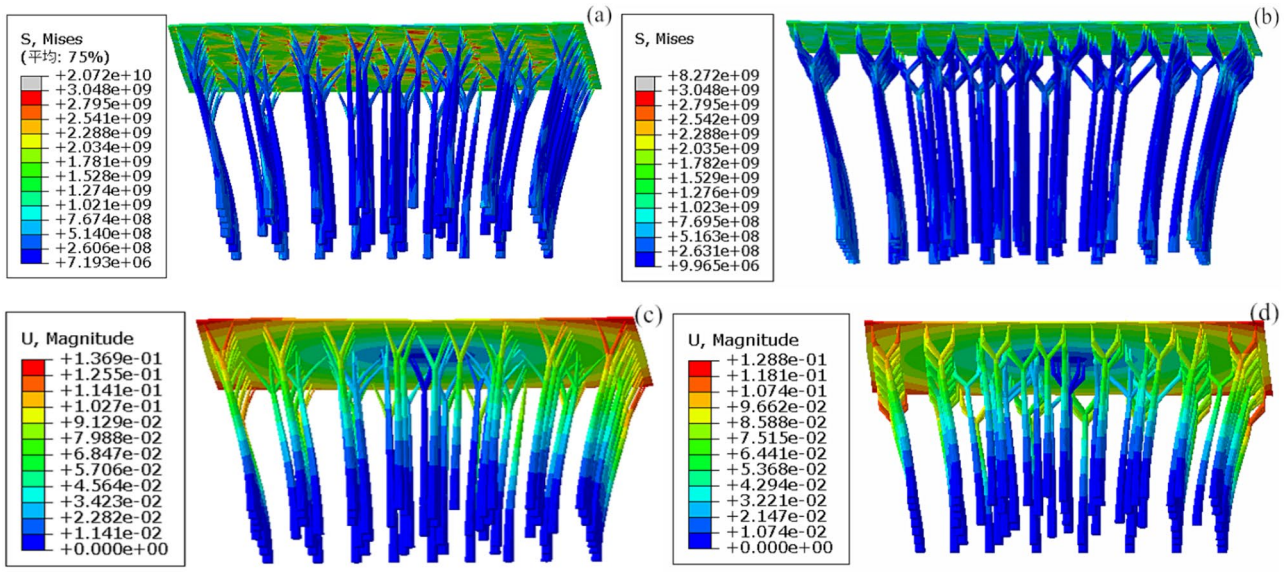

Figure 4. Stress–strain nephogram of 0.1 mm thick thin plate with different structural supports: (**a**) and (**c**) Scheme 1; (**b**) and (**d**) Scheme 2.

than those for common addition modes and Scheme 1. As shown in the displacement nephograms in Fig. 4(c) and (d), the displacement distribution areas of dendritic supports having different structural parameters were basically the same, the maximum displacements all appeared at the four corners of the 0.1 mm thin plate, and the maximum displacement of the supports also appeared at the four corners, decreasing progressively from outside to inside. The displacement magnitude was 0.137 mm for Scheme 1 and 0.129 mm for Scheme 2, with the value of the latter being slightly smaller than that of the former. This may be because the addition of a breaking point to the dendritic support in the vertical direction allowed the stress to be released more easily through horizontal deformations.

Analysis of the influence of gradient dendritic supports having different partitions on performance

Design of gradient dendritic supports having different partition numbers

To compare the influence of gradient dendritic supports having different partitions on the performances of parts, we designed a thin plate, 20 mm × 20 mm × 0.1 mm, in Magics, moved the thin plate to 10 mm above the processing platform and then independently added two dendritic supports having different parameters, as shown in Fig. 5. The support having two partitions was as follows: the diameter of conical apex was 0.1 mm, the diameter of conical base was 0.6 mm, the maximum row spacing between inner cones was 2 mm, the maximum row spacing between outer cones was 1 mm, the Z-axis offset was 0.05 mm, the maximum trunk height was 8 mm, the number of branches was 4, a breaking point was added in the vertical direction (0.3 mm in diameter and 1 mm from the top), the part volume measured 40 mm^3, and the support volume was 131.835 mm^3. The support having three partitions was as follows: the diameter of conical apex was 0.1 mm, the diameter of conical base was 0.6 mm, the maximum row spacing between inner cones was 2.5 mm, the maximum row spacing between intermediate cones was 1.8 mm, the maximum row spacing between outer cones was 1.1 mm, the Z-axis offset was 0.05 mm, the maximum trunk height was 8 mm, the number of branches was 4, a breaking point was added in the vertical direction (0.3 mm in diameter and 1 mm from the top), the part volume measured 40 mm^3, and the support volume was 125.139 mm^3.

Thermal stress analysis of gradient dendritic supports having different partition numbers

The stress and strain nephograms and temperature distribution nephograms of gradient dendritic supports having different partition numbers are shown in Fig. 6. As shown in the stress nephograms in Fig. 6(a), (c), the stress distribution areas of dendritic supports having different structural parameters all appeared at the apices of the supports, and the stress intensity decreased progressively from apex to base. The structure of a support with three partitions was more uniform than that of one with two partitions. The stress intensity distribution was $9.925e^9$ MPa for the structure with two partitions and $1.109e^{10}$MPa for the structure with three partitions, and there was little difference in the stress intensity levels. The displacement nephograms in Fig. 6(b), (d) show that the displacement distribution areas of the gradient dendritic supports having different partition numbers were basically the same, the maximum displacements all appeared at the four corners of the 0.1-mm thin plate, and the maximum displacement of the supports also appeared at the four corners, decreasing progressively from outside to inside. The displacement magnitude was 0.1342 mm for the structure having two partitions and 0.1412 mm for the structure having three partitions. The value of the structure having two partitions was slightly less than that having three partitions, probably because the latter required a slightly larger support addition. Thus, when the cross-sectional area of the part was not very big, there was not much difference between adding two or three partitions to the gradient supports of the part. A comparison of a partitioned gradient support and Scheme 2 indicated that after the former was added, the stress distribution and displacement reduction for the molded part did not improve, which may be related to the parts having fewer intermediate support additions, making it difficult for intermediate heat to dissipate, thereby forming a large temperature gradient, as shown in Fig. 6(e–g).

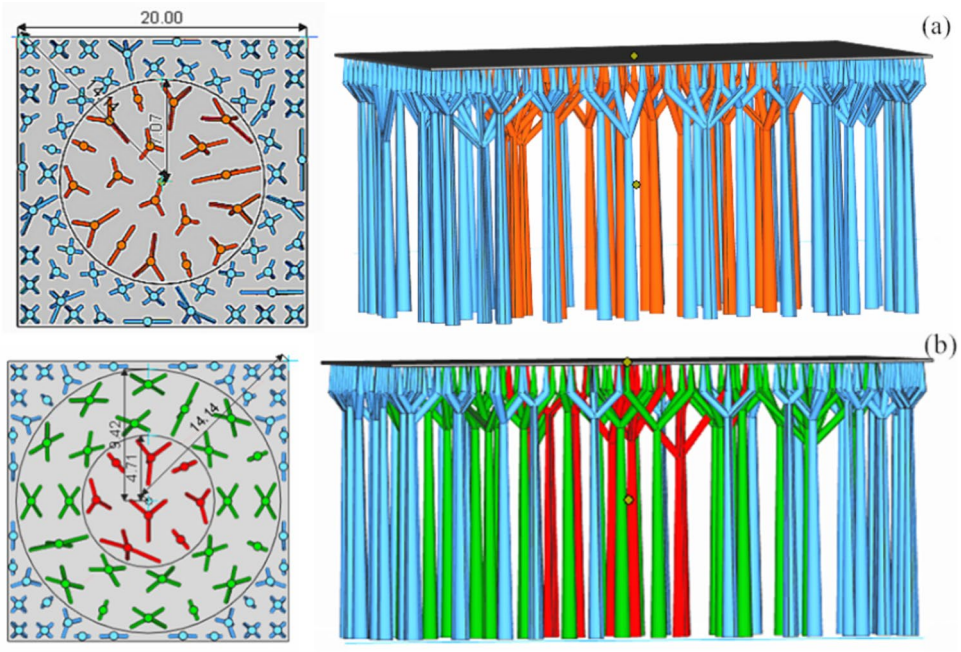

Figure 5. Schematic diagram of 0.1 mm thick thin plate adding gradient tree support in different zones: (**a**) 2 partitions; (**b**) 3 partitions.

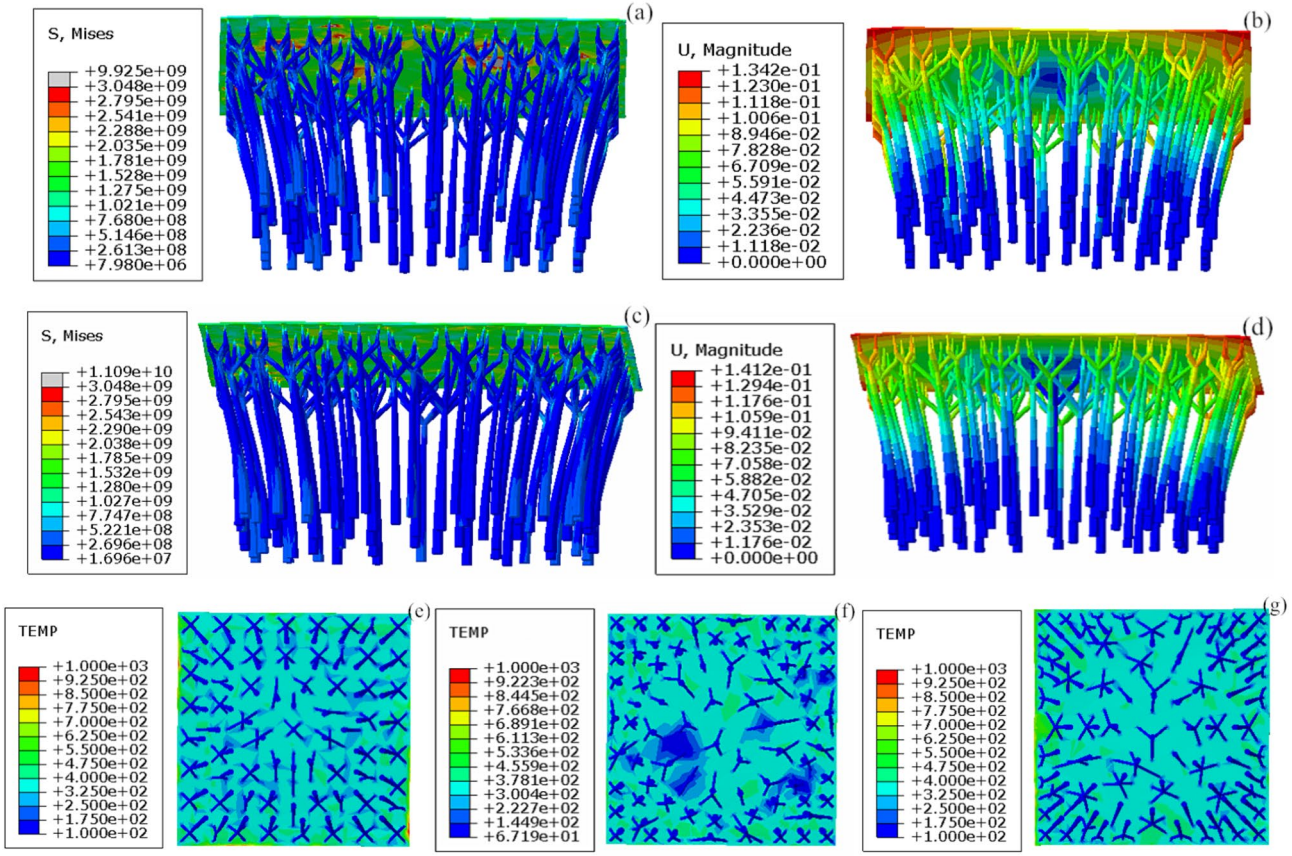

Figure 6. Finite element analysis results for a 0.1-mm thin plate with dendritic supports having different structures: (**a**), (**b**) and (**f**) represent a support with two partitions; (**c**), (**d**) and (**g**) represent a support with three partitions; (**e**) Scheme 2.

Analysis of the optimized partitioned gradient dendritic support's design

Optimized design of a dendritic gradient support

Two further investigate the factors affecting dendritic support performance, we designed a thin 20 mm × 20 mm × 0.1 mm plate in Magics, moved the thin plate to 10 mm above the processing platform and then added a gradient dendritic support, as shown in Fig. 7. The parameters of support having two partitions was as follows: the diameter of conical apex was 0.1 mm, the diameter of conical base was 0.6 mm, the maximum row spacing between inner cones was 1.6 mm, the maximum row spacing between outer cones was 1.2 mm, the Z-axis offset was 0.05 mm, the maximum trunk height was 8 mm, the number of branches was 4, a breaking point was added in the vertical direction (0.3 mm in diameter and 1 mm from the top), the part volume measured 40 mm^3, and the support volume was 145.103 mm^3.

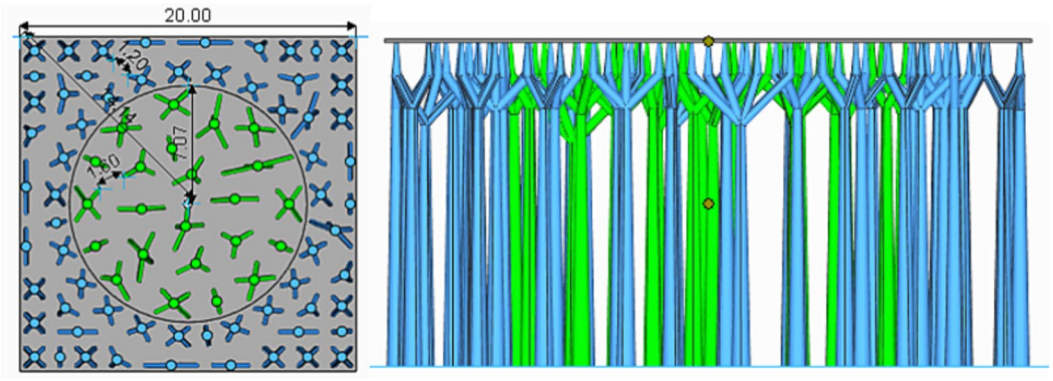

Figure 7. Schematic of the optimized design of the gradient dendritic support.

Thermal stress analysis of optimized dendritic support

The stress and strain nephograms of the optimized dendritic support are shown in Fig. 8. As shown in the stress nephogram in Fig. 8 (a), the stress of the optimized dendritic support was concentrated in the apices of the supports, the stress intensity decreased progressively from apex to base, and the stress was evenly distributed. The intensity distribution was $1.078e^9$ MPa for the optimized dendritic support, which was the equivalent to those having two partitions and Scheme 2. The displacement nephogram in Fig. 8(b) shows that the displacement distribution areas were basically the same, the maximum displacements all appeared at the four corners of the 0.1-mm thin plate, and the maximum displacement of the support also appeared at the four corners, decreasing progressively from outside to inside. The maximum displacement of parts having the optimized support was 0.118 mm, which was slightly smaller than those having two partitions and Scheme 2. This may be because the optimized dendritic support adopted a two-partition structure, and the inner support addition was the same as that of Scheme 2, which ensured heat dissipation from inside parts, whereas the outer ring increased the pulling force of the support and guaranteed the heat dissipation from outside parts by reinforcing and densifying supports.

Performance analysis of parts having different structural supports molded by SLM

Placement of parts having different supports

In the above simulation analysis, adding different structural supports beneath a 0.1-mm thin plate was performed mainly to minimize the difficulty levels of data calculations and analyses. In actual processing, owing to the processing accuracy of the laser and the improved ability to observe part deformations, we adjusted the thickness of the part to 0.5 mm, imported differently designed supporting structures into Magics software and placed them in a certain order, as shown in Fig. 9.

Performance analysis of parts molded by SLM

Parts having different structural supports molded by SLM are shown in Fig. 10. The overall morphology of the parts in Fig. 10 revealed bright and clean surfaces, as well as excellent metal textures. A comparison of the deformations of parts having conical, E-stage and dendritic supports showed that the maximum deformations occurred with a conical support, followed by a dendritic support and then an E-stage support. This suggested that an E-stage support provided the best performance, but this support type required a large support addition, as verified by the simulation in Section "Thermal stress analysis of common supports". A comparison of the deformations of parts with dendritic supports having different structural parameters (Schemes 1 and 2) showed that Scheme 1 resulted in the largest deformations, which may be because the addition of a breaking point to the dendritic support in the vertical direction allowed the stress to be released more easily through horizontal deformations. This verified the simulation results of Section "Thermal stress analysis of dendritic supports with different structural parameters". A comparison of the deformations of parts with gradient dendritic supports having different partition numbers (two or three) revealed that three partitions resulted in a larger deformation than two partitions, which indicated that when adding gradient supports of similar volumes, increasing the partitions does not improve the molding quality of the parts. By comparing the deformation of parts having

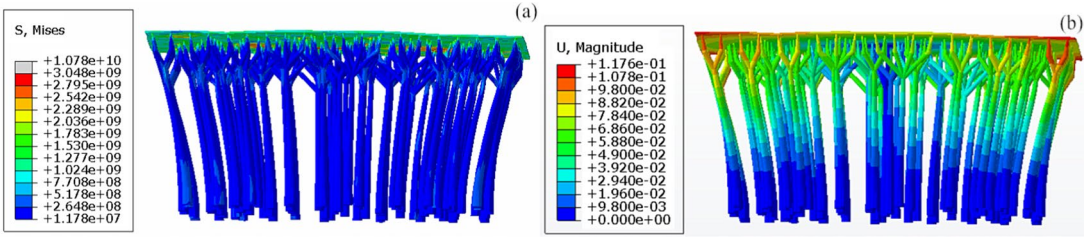

Figure 8. Finite element analysis results of tree support after optimization design: (**a**) Stress nephogram; (**b**) Strain nephogram.

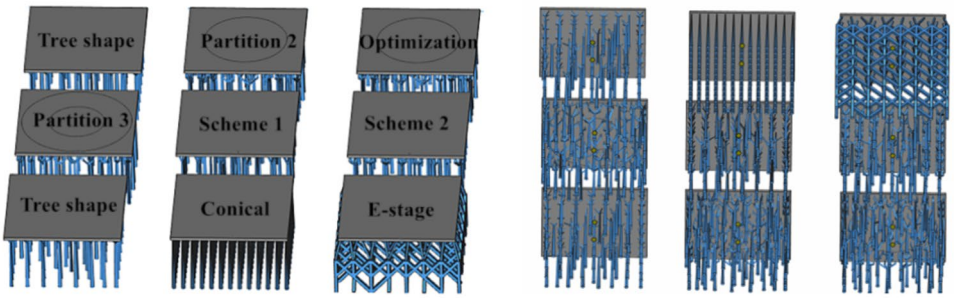

Figure 9. Arrangement sequence of supporting parts of different structures.

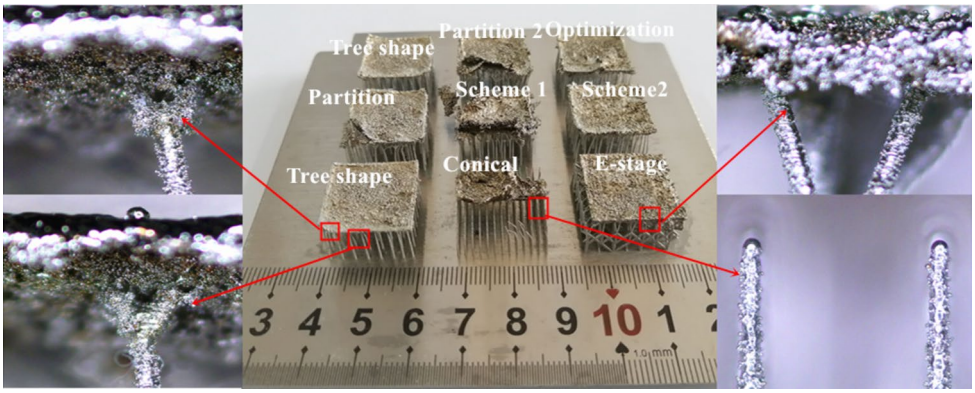

Figure 10. Part diagram of SLM forming with different structural supports.

supports (two partitions, Scheme 2 and optimized design), we found that deformations were minimized using Scheme 2, and the deformations produced using the optimized design were similar to those of the two-partition supports. The experimental results were slightly different from the simulation results, but not markedly, indicating that when adding supports of similar volumes, the addition of a gradient support to parts does not improve the molding quality. Figure 10 the microstructure of the part shows that the e-Stage support and tree support are in good contact with the part. The tree support has more powder adhesion on the branch part in contact with the part, which is mainly related to the high energy density of the branch part. The contact part between the conical support and the parts is broken, which is mainly related to the large shrinkage stress, but the forming effect of the support is good.

Conclusions

- The simulation results using a 0.1-mm thin plate having different supporting structures indicated that the maximum stress concentration occurs with a dendritic support, followed by E-stage support and then conical support. The displacement order is slightly different, being greatest for a conical support, followed by dendritic support and then E-stage support. As long as the support does not break, the E-stage support has the best performance, but it requires a large support addition.
- When dendritic supports having different structural parameters are added to parts, the stress concentration and deformation of Scheme 2 were smaller than those of Scheme 1, which may be because the addition of a breaking point in the vertical direction allows the stress to be released more easily through horizontal deformations. The simulation results of parts having gradient dendritic supports with different partition numbers (two and three) revealed that the stress intensity and deformations for two partitions were slightly smaller than those for three partitions.
- For parts with different structural supports molded by SLM, the maximum deformation occurs with a conical support, followed by a dendritic support and then an E-stage support. When gradient supports of similar volumes were added, adding partitions did not effectively improve the molding quality. When supports of similar volumes were added, adding gradient supports to parts did not effectively improve the molding quality.

Of course, follow-up studies are needed to further improve the quality of parts molded by SLM by reducing the residual stresses of molded parts by preheating the substrate, increasing the number of branches of dendritic supports, optimizing the powder-spreading structure to minimize powder dispersal when parts come into contact, changing the placement of parts to reduce the length of laser scanning line. The current study laid a foundation for the direct manufacturing of high-precision parts using SLM technology.

Data availability

The datasets used and/or analyzed during the current study are available from the corresponding author on reasonable request.

Received: 10 January 2024; Accepted: 26 July 2024
Published online: 06 August 2024

References

1. Yuan, L., Ding, S. & Wen, C. Additive manufacturing technology for porous metal implant applications and triple minimal surface structures: A review. *Bioact. Mater.* **4**, 56–70 (2019).
2. Yu, W. A. *et al.* Lattice structure design optimization coupling anisotropy and constraints of additive manufacturing. *Mater. Des.* **196**, 109089 (2020).

3. Aboulkhair, Nesma T. *et al.* 3D printing of Aluminium alloys: Additive Manufacturing of Aluminium alloys using selective laser melting. *Progress Mater. Sci.* **106**, 100578 (2019).
4. Liu, J. *et al.* Effect of scanning speed on the microstructure and mechanical behavior of 316L stainless steel fabricated by selective laser melting. *Mater. Des.* **186**, 108355 (2020).
5. Wang, D. *et al.* Research on the fabricating quality optimization of the overhanging surface in SLM process. *Int. J. Adv. Manuf. Technol.* **65**(9–12), 1471–1484 (2013).
6. Zhang H. Research on support design of selected area laser melting parts. Zhejiang University of Technology, 2018.
7. Gan, M. X. & Wong, C. H. Practical support structures for selective laser melting. *J. Mater. Process. Technol.* **238**, 474–484 (2016).
8. Tang, G., Feng, T., Duan, G., Wu, P. & Feng, Y. Simulation of metal selective laser melting. *Equip. Manuf. Technol.* **12147–153**, 165 (2018).
9. Lu, Q., Zhong, S. & Wu, J. Optimization analysis of titanium support based on SLM forming simulation. *New Technol. New Process* **1**, 62–65 (2020).
10. Chen, C., Wu, S., Ding, H. & Chen, H. Research on support addition of suspended structure by selective laser melting. *Tool Technol.* **12**, 56–59 (2019).
11. Zhang, X., Kang, J., Duan, G., Feng, T. & Rong, Y. Normal distribution support design of SLM additive manufacturing workpiece. *Hot Work. Process* **15**, 136–139 (2019).
12. Craeghs, T. *et al.* Detection of Process failures in layerwise laser melting with optical process monitoring. *Phys. Procedia* **39**, 753–759 (2012).
13. Calignano, F. Design optimization of supports for overhanging structures in aluminum and titanium alloys by selective laser melting. *Mater. Des.* **64**, 203–213 (2014).
14. Malekipour, Ehsan, Tovar, Andres & El-Mounayri, Hazim. Heat conduction and geometry topology optimization of support structure in laser-based additive manufacturing. *Mech. Addit. Adv. Manuf.* **9**, 17–27 (2018).
15. Guoqing, Zhang *et al.* Optimal design of support structures in selective laser melting of parts. *Chin. J. Lasers* **43**(12), 1202002 (2016).
16. Srinivasan, D. *et al.* 3D printing manufacturing techniques, materials, and applications: An overview. *Adv. Mater. Sci. Eng.* **2021**, 1–10 (2021).

Acknowledgements

The study was funded by the Henan Provincial Science and Technology Project (242102311240) and the Key Scientific Research Projects of Colleges and Universities in Henan Province (22A460006). Also, this work was supported by Analytical and Testing Center of ZKNUC for carrying out microscopic analysis.

Author contributions

Conceptualization: Guoqing Zhang Funding acquisition: Guoqing Zhang Investigation: Guoqing Zhang, Junxin Li, Xiaoyu Zhou Formal analysis: Guoqing Zhang, Writing – original draft: Guoqing Zhang Writing – review & editing: Guoqing Zhang , Anmin wang.

Competing interests

The authors declare no competing interests.

Additional information

Correspondence and requests for materials should be addressed to Z.G.

Reprints and permissions information is available at www.nature.com/reprints.

Publisher's note Springer Nature remains neutral with regard to jurisdictional claims in published maps and institutional affiliations.